

High activity of hot electrons from bulk 3D graphene materials for efficient photocatalytic hydrogen production

Yanhong Lu^{1,3,§}, Bo Ma^{2,§}, Yang Yang^{1,2}, Erwei Huang², Zhen Ge^{1,2}, Tengfei Zhang^{1,2}, Suling Zhang³, Landong Li² (✉), Naijia Guan², Yanfeng Ma^{1,2}, and Yongsheng Chen^{1,2} (✉)

¹State Key Laboratory and Institute of Elemento-Organic Chemistry, Collaborative Innovation Center of Chemical Science and Engineering (Tianjin), Key Laboratory of Functional Polymer Materials and the Centre of Nanoscale Science and Technology, Institute of Polymer Chemistry, College of Chemistry, Nankai University, Tianjin 300071, China

²School of Material Science and Engineering & National Institute for Advanced Materials, Nankai University, Tianjin 300350, China

³School of Chemistry & Material Science, Langfang Teachers University, Langfang 065000, China

[§] These authors contributed equally to this work.

Received: 6 October 2016
Revised: 21 November 2016
Accepted: 23 November 2016

© Tsinghua University Press
and Springer-Verlag Berlin
Heidelberg 2016

KEYWORDS

graphene,
hot electron,
hydrogen production,
water splitting,
TiO₂

ABSTRACT

Design and synthesis of efficient photocatalysts for hydrogen production via water splitting are of great importance from both theoretical and practical viewpoints. Many metal-based semiconductors have been explored for this purpose in recent decades. Here, for the first time, an entirely carbon-based material, bulk three-dimensionally cross-linked graphene (3DG), has been developed as a photocatalyst for hydrogen production. It exhibits a remarkable hydrogen production rate of $270 \mu\text{mol}\cdot\text{h}^{-1}\cdot\text{g}_{\text{cat}}^{-1}$ under full-spectrum light via a hot/free electron emission mechanism. Furthermore, when combined with the widely used semiconductor TiO₂ to form a TiO₂/3DG composite, it appears to become a more efficient hydrogen production photocatalyst. The composite achieves a production rate of $1,205 \mu\text{mol}\cdot\text{h}^{-1}\cdot\text{g}_{\text{cat}}^{-1}$ under ultraviolet–visible (UV–vis) light and a 7.2% apparent quantum efficiency at 350 nm due to the strong synergetic effects between TiO₂ and 3DG.

1 Introduction

Hydrogen is one of the most important materials in the chemical industry and a strategically appealing energy source [1]. Hydrogen is produced in large quantities. More than 50 million tons are available from fossil fuel feedstocks worldwide every year [2]. Hydrogen is expensive and both consumes non-

renewable resources and generates tremendous CO₂ emissions. Thus, great efforts have been devoted to exploring an economical and environmentally friendly process for hydrogen production. Since the pioneering study of photoelectrochemical water splitting on a TiO₂ electrode by Fujishima and Honda in the 1970s [3], solar hydrogen generation through photocatalytic water splitting has been considered a promising

Address correspondence to Yongsheng Chen, yschen99@nankai.edu.cn; Landong Li, lild@nankai.edu.cn

solution due to its energetic and environmental advantages. It therefore receives considerable attention [4–7]. Over the past 40 years, many metal-based semiconductor photocatalysts [8, 9], including metal oxides [10, 11], metal sulfides [12] or selenides [13], metal oxynitrides [14], and perovskite oxide [15], have been investigated for photocatalytic water splitting processes. The most rare and expensive metals are employed frequently in efficient semiconductor systems. Thus, alternative photocatalysts that use abundant, environmentally friendly materials for efficient hydrogen production are in high demand. With this in mind, carbon-based materials, e.g., graphitic carbon nitride [16–19] and carbon nanotubes [20, 21], have recently been investigated as metal-free semiconductor photocatalysts for water splitting.

Graphene, a typical and unique 2D carbon nano-material, has been explored as an important component of, or precursor to semiconductor photocatalysts for hydrogen evolution via water splitting. Graphene oxide (GO) [22], heteroatom-doped graphene [23–25] and graphene-based composite photocatalysts [26–30] are reported to be promising materials for semiconductor photocatalysis. When GO or heteroatom-doped graphene is used as a semiconductor photocatalyst, a semiconductor band gap is created by tuning the electronic properties and modifying the density of states of graphene through the introduction of vacancies or heteroatoms [31]. In graphene-based composite photocatalysts, graphene is used as a support or matrix material for metal-based semiconductor nanoparticles in order to enhance the transfer and separation of photogenerated electrons and holes. Graphene is a zero-bandgap semiconductor with an infinite sp^2 domain due to contact between π and anti-bonding π (π^*) orbitals at Brillouin zone corners and thus full spectrum absorption [32]. However, single sheets of graphene have not been used for photocatalytic hydrogen production thus far. Recently, it has been disclosed that graphene can achieve a unique reverse saturation state with a high density ($\sim 10^{13} \text{ cm}^{-2}$) [33] of hot electrons well above the Fermi level when under illumination with light, and that these hot electrons can even be ejected via an Auger-like mechanism [34, 35] due to the unique Dirac band structure which causes the conventional relaxation of

the excited electrons to be bottlenecked [36–38]. These highly energetic hot or ejected free electrons can be used as powerful, clean reducing agents to drive redox reactions such as atmospheric ammonia synthesis [39] and other reactions which fail via conventional methods or require harsh conditions [40–42].

In this work, for the first time, we report that a carbon-only bulk three dimensionally cross-linked graphene (3DG) material can be used as a robust catalyst for photocatalytic hydrogen production via water splitting under ultraviolet–visible (UV–vis) light using a hot electron mechanism. Furthermore, dramatically enhanced hydrogen production catalytic activity is achieved when 3DG is loaded with TiO_2 nanoparticles, due to the synergetic effects between TiO_2 and 3DG.

2 Experimental

2.1 Materials synthesis

All chemicals used in this study were of analytical grade and used directly without further purification. Distilled water was used in all experiments. The starting material, GO, was synthesized via oxidation of natural graphite powder using a modified Hummers' method according to references published elsewhere [43]. 3DG was prepared via our previous procedures [34, 35]. Typically, 15 mL of GO ethanol solution ($0.6 \text{ mg}\cdot\text{mL}^{-1}$) was sealed in a 25 mL Teflon-lined autoclave, heated to 180°C and maintained at this temperature for 12 h. The autoclave was then naturally cooled to room temperature and the as-prepared ethanol-filled intermediate product was carefully removed for a slow solvent exchange with water. After the solvent exchange process was completed, the water-filled product was first freeze-dried and then dried in a vacuum oven at 120°C for 12 h. The solid sample was annealed in Ar at 250, 450, 650, and 850°C for 2 h to obtain the final graphene materials, denoted as 3DG-250, 3DG-450, 3DG-650, and 3DG-850, respectively. For comparison, an un-annealed 3DG sample was prepared using the same experimental procedures and was labeled as 3DG-un. Several 3DG composites loaded with different quantities of TiO_2 nanoparticles, denoted as $\text{TiO}_2/3\text{DG}$, were synthesized

through a process similar to the one described above. Titanium tetraisopropoxide (TTIP, $\geq 98\%$, Sigma-Aldrich) was used as the TiO_2 precursor in the GO dispersion. In a typical process, 1.5 mmol of TTIP was dissolved in ethanol and was added dropwise under magnetic stirring to a suspension containing the desired amounts of graphene, water, and ethanol. After stirring for another 2 h, the solution was treated using the procedures applied to 3DG. The solid product was then annealed in Ar at 450°C for 2 h. The intended composite graphene concentrations were 3 wt.%, 4 wt.%, 5 wt.%, 6 wt.%, 7 wt.%, and 8 wt.%, and the corresponding final products were labeled as $\text{TiO}_2/3\text{DG}-x$, where x was 3, 4, 5, 6, 7, or 8, respectively. The exact graphene contents of the composites were measured via thermogravimetric analysis (TGA) and the results are shown in Fig. S1 in the Electronic Supplementary Material (ESM). For comparison, bare TiO_2 nanoparticles were also synthesized using the same solvothermal process, but with only titanium tetraisopropoxide as the precursor, which was then annealed at 450°C in Ar. As a reference catalyst, reduced graphene oxide (rGO) was prepared using the same solvothermal process as 3DG, while the solvothermal product was dispersed in ethanol via magnetic stirring, then filtered and thoroughly washed several times with ethanol and acetone. Finally, the collected sample was dried in a vacuum oven at 120°C for 12 h and annealed in Ar at 450°C for 2 h.

2.2 Characterization

Powder X-ray diffraction (XRD) patterns were measured on a Rigaku D/Max-2500 diffractometer with $\text{Cu K}\alpha$ radiation. Raman spectra were recorded at room temperature using a Renishaw InVia Raman spectrometer with laser excitation at 514.5 nm. UV–vis absorption spectra were investigated in diffuse reflection mode using a spectrometer (Varian Cary 300) equipped with an integrated sphere attachment and with BaSO_4 as a reference. TGA was performed on a TA SDT Q600 analyzer in air at a heating rate of $10^\circ\text{C}\cdot\text{min}^{-1}$. Scanning electron microscopy (SEM) images were obtained on a FEI NanoSem 430 field emission scanning electron microscope using an accelerating voltage of 20 kV. High resolution transmission electron

microscopy (HR-TEM) was conducted in a FEI Tecnai G² F20 electron microscope using an acceleration voltage of 200 kV. Nitrogen adsorption/desorption analysis was performed at 77 K on a Quantachrome iQ-MP gas adsorption analyzer. The specific surface area was determined using the Brunauer–Emmett–Teller (BET) method and the pore size distribution was analyzed by applying a nonlocal density functional theory method with a slit pore model to the nitrogen adsorption data. For electrochemical impedance spectroscopy (EIS) measurements, the 3DG or $\text{TiO}_2/3\text{DG}$ powders were fixed to the film electrodes via the following method: The powders and Nafion/ethanol were homogeneously mixed and then spread on the conducting fluorine-doped SnO_2 glass substrate (FTO). Finally, films with thicknesses of $\sim 2\ \mu\text{m}$ and $0.5\ \text{cm}^2$ active areas were calcinated at 450°C for 2 h in Ar. The EIS measurements were carried out on a P4000 electrochemical workstation (Princeton, USA) using a three-electrode system in an alternating current frequency range of 10 kHz to 0.01 Hz, in a 0.5 M Na_2SO_4 solution. The resulting electrode served as the working electrode. Platinum and saturated calomel electrodes (SCE) were used as the counter and reference electrodes, respectively.

2.3 Photocatalytic measurement

Photocatalytic hydrogen evolution reactions were performed at ambient temperature (25°C) in a top-irradiation vessel connected to a glass-enclosed gas circulation system (Labsolar- H_2 , Beijing Perfectlight Technology Co., Ltd.). A 200 W Xenon arc lamp (PLS-SXE) equipped with a filter (320–780 nm wavelength range) served as a light source with a fixed distance of 10 cm. The average intensity of irradiation was $\sim 160\ \text{mW}\cdot\text{cm}^{-2}$ as measured by the radiometers (UV-A 320–400 nm and FZ-A 400–1,000 nm, Photoelectric Instrument Factory of Beijing Normal University). In a typical photocatalytic experiment, 60 mg of $\text{TiO}_2/3\text{DG}$ (or 10 mg of 3DG) photocatalyst was dispersed in 100 mL of water containing 10% methanol by volume. Prior to irradiation, the system was evacuated for 30 min to remove dissolved oxygen. During the photocatalytic reaction, the solution was maintained under continuous magnetic stirring. The amount of

H₂ evolved was determined using a gas chromatograph with a thermal conductivity detector (CP-3800, Varian, nitrogen as a carrier gas and 5 Å molecular sieve column). The photocatalytic activity was measured under various intensities of light by positioning the lamp 20 cm away from the reactor and adjusting the working current (13, 15, 16, or 18 A) of the lamp. The intensities of light on the 3DG-650 or TiO₂/3DG-5 catalysts were 13, 24, 38, and 54 mW·cm⁻², respectively. The apparent quantum efficiency (QE) was measured under the same photocatalytic reaction conditions, but using monochromatic 350 nm UV light. The lamp was positioned 10 cm away from the reactor and the intensity of light on the reactor was ~3.2 mW·cm⁻² over an area of 7.1 cm². The QE was calculated using the following Eq. (1)

$$\begin{aligned} \text{QE}(\%) &= \frac{\text{Number of reacted electrons}}{\text{Number of incident photons}} \times 100 \\ &= \frac{\text{Number of evolved H}_2 \text{ molecules} \times 2}{\text{Number of incident photons}} \times 100 \end{aligned} \quad (1)$$

3 Results and discussion

3.1 Structure and properties of 3DG and TiO₂/3DG

The structures of as-synthesized bare TiO₂, 3DG-450, and TiO₂/3DG-5 composites were analyzed. As shown in the X-ray diffraction results in Fig. 1(a), clear and characteristic diffraction peaks for anatase TiO₂ (JCPDS card No. 21-1272; space group *I*₄/*amd*; *a*₀ = 3.7852 Å, *c*₀ = 9.5139 Å) are observed at about 25.3°, 37.8°, 48.0°, 53.9°, 55.1°, and 62.7°, indexed to the (101), (004), (200), (105), (211), and (204) crystal planes, respectively. In the 3DG-450 sample, the broad diffraction peak from 15° to 30° corresponds to the (002) peak of graphene [44], and its broad nature indicates poor ordering of the sheets along the stacking direction [45]. While most of the characteristic diffraction peaks of TiO₂ are observed in the composite catalyst TiO₂/3DG-5, no clear peaks from graphene are observed due to both the lower packing order of graphene sheets and their lower concentration compared to that of TiO₂ in the composite [46]. However, the presence of graphene can be clearly elucidated by Raman analysis (Fig. 1(b)).

Peaks at about 1,350 and 1,597 cm⁻¹, which correspond to the D and G bands of graphene, are clearly present in both the 3DG-450 and TiO₂/3DG-5 catalysts. Furthermore, peaks at 145, 397, 515, and 637 cm⁻¹, which arise from anatase phase TiO₂ were also clearly observed in both TiO₂ and TiO₂/3DG-5, consistent with the XRD analysis results. The optical absorption spectra of 3DG-450, bare TiO₂, and TiO₂/3DG-5 are shown in Fig. 1(c). Without an absorption edge in its absorbance spectrum, 3DG-450 exhibits the character of a zero bandgap semiconductor, which is similar to an individual graphene sheet. It exhibits absorption across the full solar spectrum as expected. While TiO₂ and TiO₂/3DG-5 show obvious absorption edges at 390 and 480 nm, respectively. TiO₂/3DG-5 exhibits a red-shift (~90 nm) relative to bare TiO₂ due to the interaction between TiO₂ and 3DG [47]. This corresponds to a bandgap reduction from 3.2 to 2.7 eV, as revealed by the plots of the Kubelka–Munk remission function in the inset of Fig. 1(c).

The morphologies of 3DG-450 and the TiO₂/3DG-5 composite are illustrated in Fig. 2. In Fig. 2(a), the bulk 3D graphene material is assembled with cross-linked individual graphene sheets, similar to our previous reports [34, 35]. With its unique structure and morphology, the 3DG material can be treated as a monolithic, cross-linked polymer but with 2D graphene sheets as a monomer which is cross-linked primarily at the edge, and with large void spaces between the individual sheets. This unique structure causes the 3DG material to retain the nature of individual graphene sheets and thus exhibit the unique, remarkable mechanical and (opto)electronic properties of graphene in the bulk state [34, 35]. The morphology of the TiO₂/3DG-5 composite changes little from the template of 3DG-450 (Fig. S2 in ESM), where TiO₂ particles are homogeneously distributed throughout the surfaces of the graphene sheets at the nanoscale (Fig. 2(b)). As the size of the photocatalyst is critical to its catalytic activity [10], the sizes of TiO₂ particles loaded onto 3DG were limited to ~10 nm (Fig. 2(c)). This was achieved using the well-known wet chemistry method for synthesis of nano-sized TiO₂ [45, 48]. As shown in Fig. 2(d), HR-TEM analysis of TiO₂ nanoparticles loaded onto graphene sheets indicates a typical anatase structure with a lattice fringe of

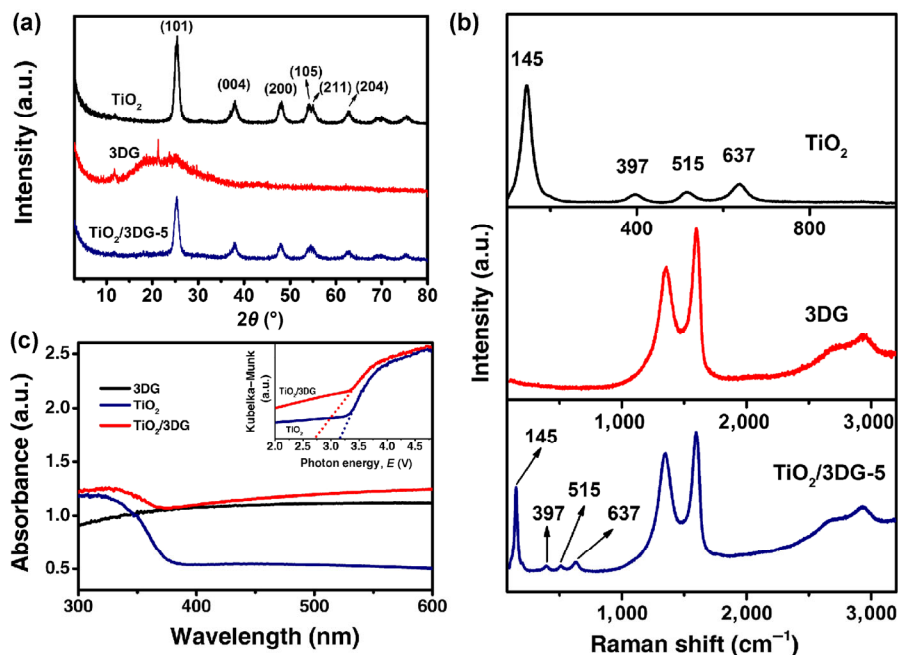


Figure 1 Structural analyses of bare TiO_2 , 3DG-450, and $\text{TiO}_2/3\text{DG-5}$ catalysts. (a) X-ray diffraction spectra, (b) Raman spectra, and (c) UV-vis absorbance spectra (converted from diffuse reflectance spectra). The inset is the Kubelka–Munk transformation of the absorption curves of bare TiO_2 and $\text{TiO}_2/3\text{DG-5}$.

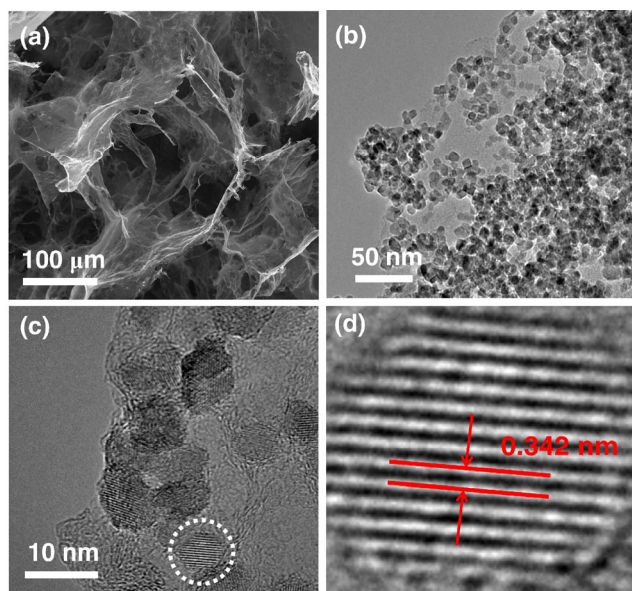


Figure 2 (a) A typical SEM image of 3DG-450 and (b) and (c) TEM and HR-TEM images of $\text{TiO}_2/3\text{DG-5}$. (d) The lattice diffraction pattern of the particle in the white circle in (c).

0.342 nm corresponding to the anatase TiO_2 (101) plane. This is consistent with the results from the XRD and Raman analyses.

The 3D porous structures of the 3DG and $\text{TiO}_2/3\text{DG}$

composites were confirmed using the BET specific surface area (SSA) and pore size distribution (PSD) analysis results. As shown in Fig. 3(a), both 3DG-450 and $\text{TiO}_2/3\text{DG-5}$ exhibit adsorption isotherms of type IV with an H_2 -type hysteresis, suggesting the presence of both mesopores and macropores. For 3DG-450, a SSA of $240 \text{ m}^2\cdot\text{g}^{-1}$ and pore volume of $0.318 \text{ cm}^3\cdot\text{g}^{-1}$ were obtained (Fig. 3(a)). From the PSD analysis (Fig. 3(b)), a sharp peak at $\sim 4 \text{ nm}$ and a broad peak ranging from 100 to 300 nm could be identified, corresponding to the inner cavities in the graphene sheets and the cage pores formed between the graphene sheets [18]. In $\text{TiO}_2/3\text{DG-5}$, because of the low loading of graphene, the pore structure is mainly composed of mesoporous (\sim tens of nm) pores with a higher pore volume ($0.467 \text{ cm}^3\cdot\text{g}^{-1}$, Fig. 3(b), square symbols). Furthermore, due to the higher density of TiO_2 nanoparticles, the SSA of the composite $\text{TiO}_2/3\text{DG-5}$ ($151 \text{ m}^2\cdot\text{g}^{-1}$) is lower than 3DG-450, but still distinctly higher than the bare TiO_2 ($91 \text{ m}^2\cdot\text{g}^{-1}$). The larger SSAs of 3DG and $\text{TiO}_2/3\text{DG}$ composites relative to those of bare TiO_2 nanoparticles and some reported photocatalysts [18, 26, 49] should be beneficial to the photocatalytic performance.

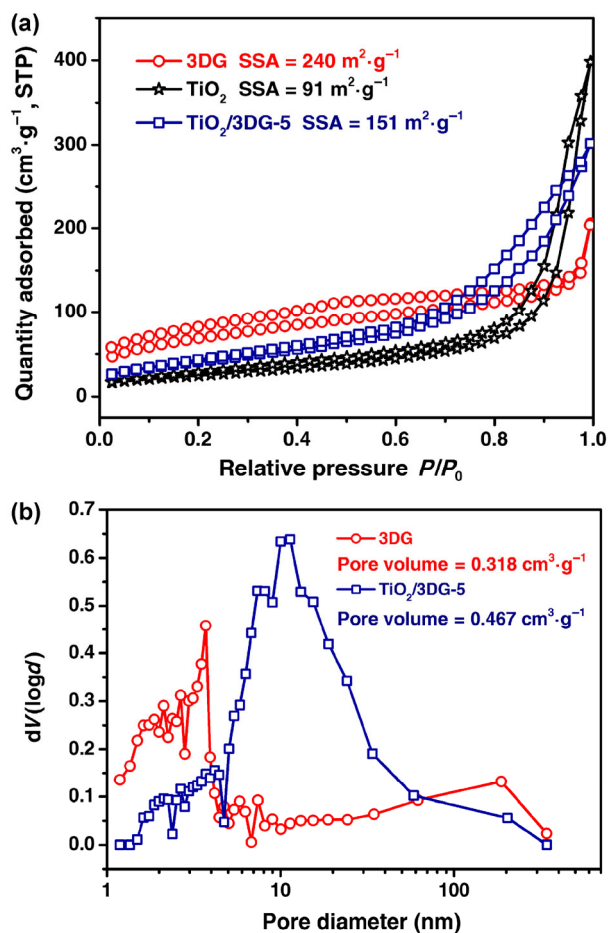


Figure 3 (a) Nitrogen adsorption–desorption isotherms of bare TiO₂, 3DG-450, and TiO₂/3DG-5. (b) Pore size distribution curves of 3DG-450 and TiO₂/3DG-5.

3.2 Photocatalytic performance

The photocatalytic hydrogen production activities of the 3DG and TiO₂/3DG composites were investigated and the results are summarized in Fig. 4. As shown in Fig. 4(a), all of the 3DG catalysts made at various annealing temperatures are active for H₂ evolution via water splitting under UV–vis light. The 3DG samples demonstrate photocatalytic activity that increases with the annealing temperature. The sample annealed at 650 °C, i.e., 3DG-650, exhibits the highest hydrogen evolution rate of 270 μmol·h⁻¹·g_{cat}⁻¹, which is much higher than those of bare TiO₂ (68 μmol·h⁻¹·g_{cat}⁻¹) or the commercial P25 TiO₂ (92 μmol·h⁻¹·g_{cat}⁻¹) under the same conditions. However, the hydrogen evolution rate of 3DG decreases with further increases in the annealing temperature, probably due to the collapse of the three dimensional structure. Only trace hydrogen could

be generated under the same conditions when using rGO as a reference photocatalyst.

Further photocatalytic studies were focused on the TiO₂/3DG composites. Surprisingly, Fig. 4(b) shows that the catalytic performances of TiO₂/3DG composite catalysts with different graphene loadings all exhibit significantly higher activity than either the bare TiO₂ or 3DG samples under the same conditions due to synergistic effects between TiO₂ and 3DG. Typically, TiO₂/3DG with a 5 wt.% loading of graphene exhibits the highest hydrogen evolution rate of 1,205 μmol·h⁻¹·g_{cat}⁻¹ under UV–vis light. This appears to be much higher than reported with graphene-based TiO₂ composites [50–54]. Upon increasing the graphene loading beyond 5 wt.%, the photocatalytic activity of TiO₂/3DG decreases significantly. This is probably because of the light shielding effects of graphene [54, 55]. The apparent QE is calculated to be as high as 7.2% for the optimized TiO₂/3DG-5 photocatalyst under monochromatic 350 nm UV light.

The photocatalytic nature of H₂ evolution via water splitting over 3DG-650 and TiO₂/3DG-5 is further demonstrated in Fig. 4(c), where the impact of incident light intensity on the photocatalytic activity is investigated. The catalytic activities of both 3DG-650 and TiO₂/3DG-5 photocatalysts increase linearly with the incident light intensity, consistent with the fact that the ejected hot/free electrons (measured as current) from graphene increase linearly with the light intensity [35]. These observations clearly indicate that the hot/free electrons from 3DG act as the actual reducing agent in H₂ evolution.

A typical time course of H₂ evolution via water splitting on 3DG-650 and TiO₂/3DG-5 photocatalysts under UV–vis light is shown in Fig. 4(d). The 3DG-650 and TiO₂/3DG-5 photocatalysts produce 1,435 and 6,451 μmol of hydrogen per gram, respectively, in the first 5 h under UV–vis irradiation. The amount of H₂ generated remains virtually unchanged for the next four cycles, confirming the good stability of 3DG-650 and TiO₂/3DG-5 in photocatalytic reactions, and demonstrating their potential for future applications.

3.3 Hydrogen evolution mechanism

Based on the results above, a possible mechanism of H₂ production over 3DG and TiO₂/3DG is proposed

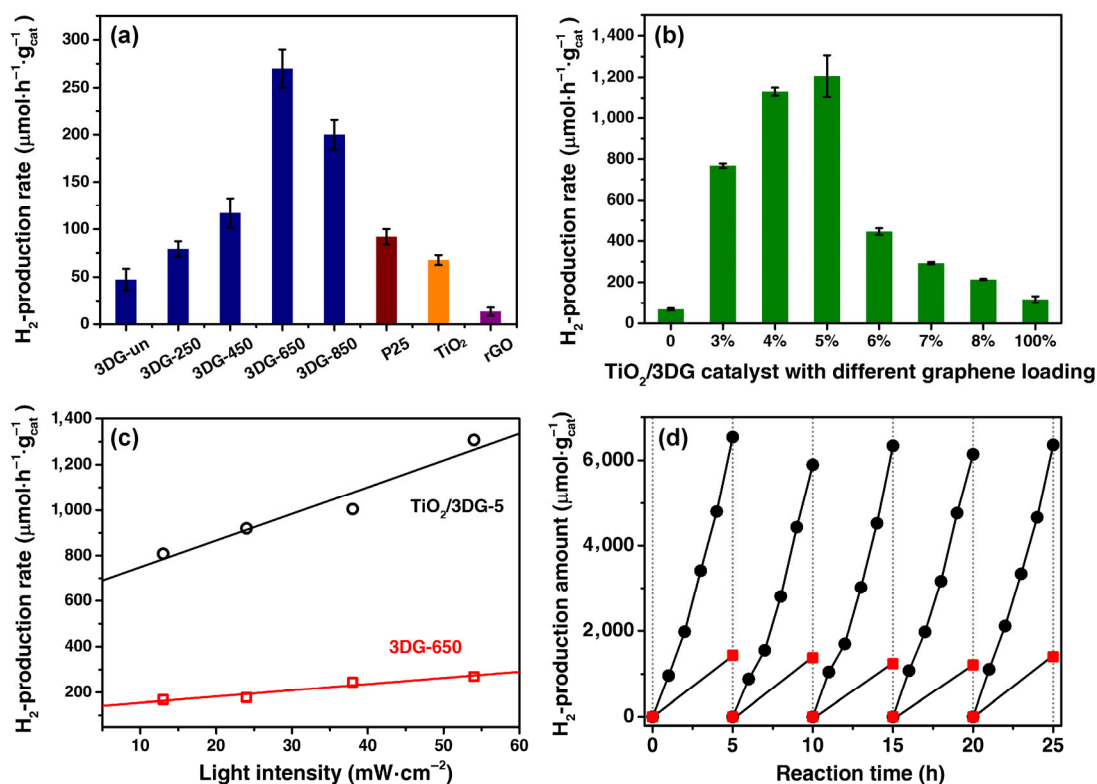


Figure 4 (a) Photocatalytic hydrogen evolution from water splitting over a series of 3DG samples synthesized at various annealing temperatures and reference samples, including bare TiO₂, commercial P25 TiO₂, and rGO. (b) TiO₂/3DG catalysts with various graphene loadings. The indicators “0” and “100%” represent bare TiO₂ and 3DG-450, respectively. (c) The relationship between H₂ production rate and light intensity using the 3DG-650 and TiO₂/3DG-5 catalysts. (d) Time course of water splitting on the TiO₂/3DG-5 (circle) and 3DG-650 (square) catalysts. The reaction proceeded for 25 h, with evacuation every 5 h (dotted line). Reaction conditions: 10 mg of 3DG or 60 mg of TiO₂/3DG composite catalyst, 90 mL of H₂O and 10 mL of methanol, and a 200 W Xe lamp with a 320–780 nm wavelength range as the light source. The quantity of evolved H₂ was measured using a gas chromatograph with a thermal conductivity detector.

and illustrated in Fig. 5. It has been reported that hot/free electrons can be generated efficiently by graphene and 3DG materials [35, 39], and that these electrons can act as clean, powerful reducing agents for water. This is similar to the case of hot electrons ejected from plasmonic Au nanorods loaded onto MoS₂ for electrocatalytic hydrogen evolution [42]. As shown in Fig. 5(a), these highly energetic hot/free electrons can be ejected from graphene into free space via an Auger-like mechanism under light illumination. The electrons behave as massless Dirac fermions [35, 39, 56], and thus act as powerful reducing agents which drive the initial photo-reduction process of water splitting for hydrogen evolution. Meanwhile, the potential induced on graphene can drive the counter oxidation process with methanol as the sacrificial agent [57]. In our experiments without any

sacrificial agent, 3DG-650 can catalyze the splitting of pure water with a hydrogen evolution rate of 5.2 μmol·h⁻¹·g_{cat}⁻¹. This indicates a suitable redox potential of photogenerated electron–hole pairs for both water reduction and oxidation. There may be several pathways for hydrogen production using the greatly enhanced photocatalytic activity of the TiO₂/3DG composite (Fig. 5(b)). First, the 3DG in TiO₂/3DG may work as a simple photocatalyst like bare 3DG, where hot/free electrons generated under illumination with light directly reduce water to hydrogen (Fig. 5(b), path 1). In the second possible path, the photo-generated electrons transfer at the interface of graphene and TiO₂, where both electron transfer and energy transfer occur several times faster than electron–phonon energy relaxation [42, 58, 59]. Under illumination with light, the absorbed photons excite the electrons from the

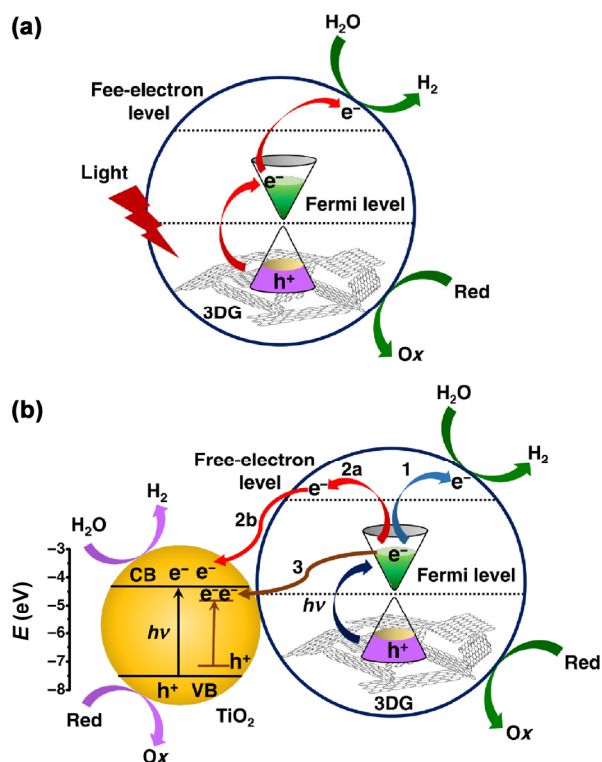


Figure 5 Pathways of electron transfer and mechanism of photocatalytic hydrogen production catalyzed by (a) 3DG and (b) $\text{TiO}_2/3\text{DG}$ catalysts.

3DG ground state, located within the TiO_2 energy gap, to an excited state that is in resonance with the TiO_2 conduction band. This can increase the TiO_2 electron density and thus greatly enhance its photocatalytic activity (Fig. 5(b), paths 2a and 2b). This charge transfer effect is supported experimentally by the EIS results. As shown in Fig. S3 in the ESM, the smaller semicircle in the Nyquist plot of $\text{TiO}_2/3\text{DG}$ -5 indicates an effective separation of photogenerated electron-hole pairs and fast interfacial charge transfer to the electron donor or acceptor. In the third possible path, the presence of 3DG can reduce the bandgap of anatase TiO_2 from 3.2 to 2.8 eV as discussed above (Fig. 1(c)) and therefore, increase the electron transfer (Fig. 5(b), path 3) from the Fermi level of 3DG to the lower conduction band of TiO_2 and suppress the recombination of photogenerated electron-hole pairs. This improves the performance of the photocatalyst accordingly [27, 59, 60]. Because of these three possible pathways for electron transfer via hot/free electron mechanisms, synergistic effects between TiO_2 and graphene should be present. These accordingly lead to the greatly

enhanced photocatalytic activity of the $\text{TiO}_2/3\text{DG}$ composite (Fig. 4(b)). A remarkably high apparent QE of 7.2% is obtained using optimized $\text{TiO}_2/3\text{DG}$ under monochromatic 350 nm UV light. This QE is significantly higher than those of other photocatalyst systems under same conditions (Table S1 in the ESM).

4 Conclusions

In summary, a bulk three dimensional graphene material has been successfully used as an efficient all-carbon photocatalyst for hydrogen evolution via water splitting under full spectrum sunlight, using a unique hot/free electron mechanism. Furthermore, dramatically enhanced photocatalytic activity is achieved using the 3DG/ TiO_2 composite catalyst. The catalyst produces 1,205 μmol of hydrogen per hour per gram of catalyst under such illumination. A high apparent QE of 7.2% is achieved using the optimized $\text{TiO}_2/3\text{DG}$ under 350 nm monochromatic UV light. This is more than an order of magnitude higher than with bare 3DG and TiO_2 . This work should offer a new strategy for overcoming the high energy barriers of many important reactions currently performed under harsh or extreme conditions, such as ammonia synthesis and CO_2 fixation.

Acknowledgements

The authors acknowledge the financial support from the Ministry of Science and Technology of China (No. 2016YFA0200200), the National Natural Science Foundation of China (Nos. 51633002, 51472124, 51273093, and 51502125), the Natural Science Foundation of Hebei Province of China (No. E2016408035), and Science Research Project of Langfang Teachers University (No. LSLB201401).

Electronic Supplementary Material: Supplementary material (thermogravimetric analysis, optical photographs of 3DG and $\text{TiO}_2/3\text{DG}$ composite, and the comparison results of the photocatalytic hydrogen production performance between this work and the reported works) is available in the online version of this article at <http://dx.doi.org/10.1007/s12274-016-1390-5>.

References

- [1] Carraro, G.; Maccato, C.; Gasparotto, A.; Montini, T.; Turner, S.; Lebedev, O. I.; Gombac, V.; Adami, G.; Van Tendeloo, G.; Barreca, D. et al. Enhanced hydrogen production by photoreforming of renewable oxygenates through nanostructured Fe₂O₃ polymorphs. *Adv. Funct. Mater.* **2014**, *24*, 372–378.
- [2] Turner, J. A. A nickel finish protects silicon photoanodes for water splitting. *Science* **2013**, *342*, 811–812.
- [3] Fujishima, A.; Honda, K. Electrochemical photolysis of water at a semiconductor electrode. *Nature* **1972**, *238*, 37–38.
- [4] Reece, S. Y.; Hamel, J. A.; Sung, K.; Jarvi, T. D.; Esswein, A. J.; Pijpers, J. J.; Nocera, D. G. Wireless solar water splitting using silicon-based semiconductors and earth-abundant catalysts. *Science* **2011**, *334*, 645–648.
- [5] Kenney, M. J.; Gong, M.; Li, Y. G.; Wu, J. Z.; Feng, J.; Lanza, M.; Dai, H. J. High-performance silicon photoanodes passivated with ultrathin nickel films for water oxidation. *Science* **2013**, *342*, 836–840.
- [6] Li, J.-S.; Wang, Y.; Liu, C.-H.; Li, S.-L.; Wang, Y.-G.; Dong, L.-Z.; Dai, Z.-H.; Li, Y.-F.; Lan, Y.-Q. Coupled molybdenum carbide and reduced graphene oxide electrocatalysts for efficient hydrogen evolution. *Nat. Commun.* **2016**, *7*, 11204.
- [7] Muhich, C. L.; Evanko, B. W.; Weston, K. C.; Lichty, P.; Liang, X. H.; Martinek, J.; Musgrave, C. B.; Weimer, A. W. Efficient generation of H₂ by splitting water with an isothermal redox cycle. *Science* **2013**, *341*, 540–542.
- [8] Chen, X. B.; Shen, S. H.; Guo, L. J.; Mao, S. S. Semiconductor-based photocatalytic hydrogen generation. *Chem. Rev.* **2010**, *110*, 6503–6570.
- [9] Lu, Q. P.; Yu, Y. F.; Ma, Q. L.; Chen, B.; Zhang, H. 2D transition-metal-dichalcogenide-nanosheet-based composites for photocatalytic and electrocatalytic hydrogen evolution reactions. *Adv. Mater.* **2016**, *28*, 1917–1933.
- [10] Murdoch, M.; Waterhouse, G. I. N.; Nadeem, M. A.; Metson, J. B.; Keane, M. A.; Howe, R. F.; Llorca, J.; Idriss, H. The effect of gold loading and particle size on photocatalytic hydrogen production from ethanol over Au/TiO₂ nanoparticles. *Nat. Chem.* **2011**, *3*, 489–492.
- [11] Yu, J. G.; Ran, J. R. Facile preparation and enhanced photocatalytic H₂-production activity of Cu(OH)₂ cluster modified TiO₂. *Energy Environ. Sci.* **2011**, *4*, 1364–1371.
- [12] Zhang, J.; Yu, J. G.; Zhang, Y. M.; Li, Q.; Gong, J. R. Visible light photocatalytic H₂-production activity of CuS/ZnS porous nanosheets based on photoinduced interfacial charge transfer. *Nano Lett.* **2011**, *11*, 4774–4779.
- [13] Han, Z. J.; Qiu, F.; Eisenberg, R.; Holland, P. L.; Krauss, T. D. Robust photogeneration of H₂ in water using semiconductor nanocrystals and a nickel catalyst. *Science* **2012**, *338*, 1321–1324.
- [14] Maeda, K.; Teramura, K.; Lu, D. L.; Takata, T.; Saito, N.; Inoue, Y.; Domen, K. Photocatalyst releasing hydrogen from water. *Nature* **2006**, *440*, 295.
- [15] Suntivich, J.; May, K. J.; Gasteiger, H. A.; Goodenough, J. B.; Shao-Horn, Y. A perovskite oxide optimized for oxygen evolution catalysis from molecular orbital principles. *Science* **2011**, *334*, 1383–1385.
- [16] Wang, X. C.; Maeda, K.; Thomas, A.; Takanabe, K.; Xin, G.; Carlsson, J. M.; Domen, K.; Antonietti, M. A metal-free polymeric photocatalyst for hydrogen production from water under visible light. *Nat. Mater.* **2009**, *8*, 76–80.
- [17] Liu, J.; Liu, Y.; Liu, N. Y.; Han, Y. Z.; Zhang, X.; Huang, H.; Lifshitz, Y.; Lee, S.-T.; Zhong, J.; Kang, Z. H. Metal-free efficient photocatalyst for stable visible water splitting via a two-electron pathway. *Science* **2015**, *347*, 970–974.
- [18] Liang, Q. H.; Li, Z. L.; Yu, X. L.; Huang, Z.-H.; Kang, F. Y.; Yang, Q.-H. Macroscopic 3D porous graphitic carbon nitride monolith for enhanced photocatalytic hydrogen evolution. *Adv. Mater.* **2015**, *27*, 4634–4639.
- [19] Ong, W.-J.; Tan, L.-L.; Ng, Y. H.; Yong, S.-T.; Chai, S.-P. Graphitic carbon nitride (g-C₃N₄)-based photocatalysts for artificial photosynthesis and environmental remediation: Are we a step closer to achieving sustainability? *Chem. Rev.* **2016**, *116*, 7159–7329.
- [20] Cui, W.; Liu, Q.; Cheng, N. Y.; Asiri, A. M.; Sun, X. P. Activated carbon nanotubes: A highly-active metal-free electrocatalyst for hydrogen evolution reaction. *Chem. Commun.* **2014**, *50*, 9340–9342.
- [21] Xie, K.; Wu, H. P.; Meng, Y. N.; Lu, K.; Wei, Z. X.; Zhang, Z. Poly(3,4-dinitrothiophene)/SWCNT composite as a low overpotential hydrogen evolution metal-free catalyst. *J. Mater. Chem. A* **2015**, *3*, 78–82.
- [22] Yeh, T.-F.; Syu, J.-M.; Cheng, C.; Chang, T.-H.; Teng, H. Graphite oxide as a photocatalyst for hydrogen production from water. *Adv. Funct. Mater.* **2010**, *20*, 2255–2262.
- [23] Lavorato, C.; Primo, A.; Molinari, R.; Garcia, H. N-doped graphene derived from biomass as a visible-light photocatalyst for hydrogen generation from water/methanol mixtures. *Chem.—Eur. J.* **2014**, *20*, 187–194.
- [24] Yeh, T.-F.; Teng, C.-Y.; Chen, S.-J.; Teng, H. Nitrogen-doped graphene oxide quantum dots as photocatalysts for overall water-splitting under visible light illumination. *Adv. Mater.* **2014**, *26*, 3297–3303.
- [25] Latorre-Sánchez, M.; Primo, A.; García, H. P-doped graphene obtained by pyrolysis of modified alginate as a photocatalyst for hydrogen generation from water-methanol mixtures. *Angew. Chem., Int. Ed.* **2013**, *52*, 11813–11816.

- [26] Li, Q.; Guo, B. D.; Yu, J. G.; Ran, J. R.; Zhang, B. H.; Yan, H. J.; Gong, J. R. Highly efficient visible-light-driven photocatalytic hydrogen production of CdS-cluster-decorated graphene nanosheets. *J. Am. Chem. Soc.* **2011**, *133*, 10878–10884.
- [27] Lightcap, I. V.; Kosel, T. H.; Kamat, P. V. Anchoring semiconductor and metal nanoparticles on a two-dimensional catalyst mat. Storing and shuttling electrons with reduced graphene oxide. *Nano Lett.* **2010**, *10*, 577–583.
- [28] Xiang, Q. J.; Yu, J. G.; Jaroniec, M. Synergetic effect of MoS₂ and graphene as cocatalysts for enhanced photocatalytic H₂ production activity of TiO₂ nanoparticles. *J. Am. Chem. Soc.* **2012**, *134*, 6575–6578.
- [29] Iwashina, K.; Iwase, A.; Ng, Y. H.; Amal, R.; Kudo, A. Z-schematic water splitting into H₂ and O₂ using metal sulfide as a hydrogen-evolving photocatalyst and reduced graphene oxide as a solid-state electron mediator. *J. Am. Chem. Soc.* **2015**, *137*, 604–607.
- [30] Mateo, D.; Esteve-Adell, I.; Albero, J.; Royo, J. F. S.; Primo, A.; Garcia, H. 111 oriented gold nanoplatelets on multilayer graphene as visible light photocatalyst for overall water splitting. *Nat. Commun.* **2016**, *7*, 11819.
- [31] Deng, D. H.; Novoselov, K. S.; Fu, Q.; Zheng, N. F.; Tian, Z. Q.; Bao, X. H. Catalysis with two-dimensional materials and their heterostructures. *Nat. Nanotechnol.* **2016**, *11*, 218–230.
- [32] Castro Neto, A. H.; Guinea, F.; Peres, N. M. R.; Novoselov, K. S.; Geim, A. K. The electronic properties of graphene. *Rev. Mod. Phys.* **2009**, *81*, 109–162.
- [33] Brida, D.; Tomadin, A.; Manzoni, C.; Kim, Y. J.; Lombardo, A.; Milana, S.; Nair, R. R.; Novoselov, K. S.; Ferrari, A. C.; Cerullo, G. et al. Ultrafast collinear scattering and carrier multiplication in graphene. *Nat. Commun.* **2013**, *4*, 1987.
- [34] Wu, Y. P.; Yi, N. B.; Huang, L.; Zhang, T. F.; Fang, S. L.; Chang, H. C.; Li, N.; Oh, J.; Lee, J. A.; Kozlov, M. et al. Three-dimensionally bonded spongy graphene material with super compressive elasticity and near-zero poisson's ratio. *Nat. Commun.* **2015**, *6*, 6141.
- [35] Zhang, T. F.; Chang, H. C.; Wu, Y. P.; Xiao, P. S.; Yi, N. B.; Lu, Y. H.; Ma, Y. F.; Huang, Y.; Zhao, K.; Yan, X.-Q. et al. Macroscopic and direct light propulsion of bulk graphene material. *Nat. Photonics* **2015**, *9*, 471–476.
- [36] Tielrooij, K. J.; Song, J. C. W.; Jensen, S. A.; Centeno, A.; Pesquera, A.; Zurutuza Elorza, A.; Bonn, M.; Levitov, L. S.; Koppens, F. H. L. Photoexcitation cascade and multiple hot-carrier generation in graphene. *Nat. Phys.* **2013**, *9*, 248–252.
- [37] Zhang, L. H.; Zhu, D.; Nathanson, G. M.; Hamers, R. J. Selective photoelectrochemical reduction of aqueous CO₂ to CO by solvated electrons. *Angew. Chem., Int. Ed.* **2014**, *53*, 9746–9750.
- [38] Matsuishi, S.; Toda, Y.; Miyakawa, M.; Hayashi, K.; Kamiya, T.; Hirano, M.; Tanaka, I.; Hosono, H. High-density electron anions in a nanoporous single crystal: [Ca₂₄Al₂₈O₆₄]⁴⁺(4e⁻). *Science* **2003**, *301*, 626–629.
- [39] Lu, Y. H.; Yang, Y.; Zhang, T. F.; Ge, Z.; Chang, H. C.; Xiao, P. S.; Xie, Y. Y.; Hua, L.; Li, Q. Y.; Li, H. Y. et al. Photoprompted hot electrons from bulk cross-linked graphene materials and their efficient catalysis for atmospheric ammonia synthesis. *ACS Nano* **2016**, *10*, 10507–10515.
- [40] Kitano, M.; Inoue, Y.; Yamazaki, Y.; Hayashi, F.; Kanbara, S.; Matsuishi, S.; Yokoyama, T.; Kim, S.-W.; Hara, M.; Hosono, H. Ammonia synthesis using a stable electride as an electron donor and reversible hydrogen store. *Nat. Chem.* **2012**, *4*, 934–940.
- [41] Mukherjee, S.; Libisch, F.; Large, N.; Neumann, O.; Brown, L. V.; Cheng, J.; Lassiter, J. B.; Carter, E. A.; Nordlander, P.; Halas, N. J. Hot electrons do the impossible: Plasmon-induced dissociation of H₂ on Au. *Nano Lett.* **2013**, *13*, 240–247.
- [42] Shi, Y.; Wang, J.; Wang, C.; Zhai, T.-T.; Bao, W.-J.; Xu, J.-J.; Xia, X.-H.; Chen, H.-Y. Hot electron of Au nanorods activates the electrocatalysis of hydrogen evolution on MoS₂ nanosheets. *J. Am. Chem. Soc.* **2015**, *137*, 7365–7370.
- [43] Becerril, H. A.; Mao, J.; Liu, Z. F.; Stoltenberg, R. M.; Bao, Z.; Chen, Y. S. Evaluation of solution-processed reduced graphene oxide films as transparent conductors. *ACS Nano* **2008**, *2*, 463–470.
- [44] Tang, L. H.; Wang, Y.; Li, Y. M.; Feng, H. B.; Lu, J.; Li, J. H. Preparation, structure, and electrochemical properties of reduced graphene sheet films. *Adv. Funct. Mater.* **2009**, *19*, 2782–2789.
- [45] Shen, J. F.; Yan, B.; Shi, M.; Ma, H. W.; Li, N.; Ye, M. X. One step hydrothermal synthesis of TiO₂-reduced graphene oxide sheets. *J. Mater. Chem.* **2011**, *21*, 3415–3421.
- [46] Huang, Q. W.; Tian, S. Q.; Zeng, D. W.; Wang, X. X.; Song, W. L.; Li, Y. Y.; Xiao, W.; Xie, C. S. Enhanced photocatalytic activity of chemically bonded TiO₂/graphene composites based on the effective interfacial charge transfer through the C–Ti bond. *ACS Catal.* **2013**, *3*, 1477–1485.
- [47] Lee, J. S.; You, K. H.; Park, C. B. Highly photoactive, low bandgap TiO₂ nanoparticles wrapped by graphene. *Adv. Mater.* **2012**, *24*, 1084–1088.
- [48] Qiu, B. C.; Xing, M. Y.; Zhang, J. L. Mesoporous TiO₂ nanocrystals grown *in situ* on graphene aerogels for high photocatalysis and lithium-ion batteries. *J. Am. Chem. Soc.* **2014**, *136*, 5852–5855.
- [49] Ren, R.; Wen, Z. H.; Cui, S. M.; Hou, Y.; Guo, X. R.; Chen,

- J. H. Controllable synthesis and tunable photocatalytic properties of Ti³⁺-doped TiO₂. *Sci. Rep.* **2015**, *5*, 10714.
- [50] Li, N.; Liu, G.; Zhen, C.; Li, F.; Zhang, L. L.; Cheng, H.-M. Battery performance and photocatalytic activity of mesoporous anatase TiO₂ nanospheres/graphene composites by template-free self-assembly. *Adv. Funct. Mater.* **2011**, *21*, 1717–1722.
- [51] Zhang, X.-Y.; Li, H.-P.; Cui, X.-L.; Lin, Y. H. Graphene/TiO₂ nanocomposites: Synthesis, characterization and application in hydrogen evolution from water photocatalytic splitting. *J. Mater. Chem.* **2010**, *20*, 2801–2806.
- [52] Min, S. X.; Wang, F.; Lu, G. X. Graphene-induced spatial charge separation for selective water splitting over TiO₂ photocatalyst. *Catal. Commun.* **2016**, *80*, 28–32.
- [53] Mou, Z. G.; Wu, Y. J.; Sun, J. H.; Yang, P.; Du, Y. K.; Lu, C. TiO₂ nanoparticles-functionalized N-doped graphene with superior interfacial contact and enhanced charge separation for photocatalytic hydrogen generation. *ACS Appl. Mater. Interfaces* **2014**, *6*, 13798–13806.
- [54] Kim, H.-I.; Kim, S.; Kang, J.-K.; Choi, W. Graphene oxide embedded into TiO₂ nanofiber: Effective hybrid photocatalyst for solar conversion. *J. Catal.* **2014**, *309*, 49–57.
- [55] Chang, K.; Mei, Z. W.; Wang, T.; Kang, Q.; Ouyang, S. X.; Ye, J. H. MoS₂/graphene cocatalyst for efficient photocatalytic H₂ evolution under visible light irradiation. *ACS Nano* **2014**, *8*, 7078–7087.
- [56] Winzer, T.; Knorr, A.; Malic, E. Carrier multiplication in graphene. *Nano Lett.* **2010**, *10*, 4839–4843.
- [57] Xu, X. X.; Random, C.; Efstathiou, P.; Irvine, J. T. S. A red metallic oxide photocatalyst. *Nat. Mater.* **2012**, *11*, 595–598.
- [58] Long, R.; English, N. J.; Prezhdo, O. V. Photo-induced charge separation across the graphene–TiO₂ interface is faster than energy losses: A time-domain *ab initio* analysis. *J. Am. Chem. Soc.* **2012**, *134*, 14238–14248.
- [59] Manga, K. K.; Zhou, Y.; Yan, Y. L.; Loh, K. P. Multilayer hybrid films consisting of alternating graphene and titania nanosheets with ultrafast electron transfer and photoconversion properties. *Adv. Funct. Mater.* **2009**, *19*, 3638–3643.
- [60] Yan, Y.; Wang, C.; Yan, X.; Xiao, L. S.; He, J. H.; Gu, W.; Shi, W. D. Graphene acting as surface phase junction in anatase–graphene–rutile heterojunction photocatalysts for H₂ production from water splitting. *J. Phys. Chem. C* **2014**, *118*, 23519–23526.